Remote Sens. **2009**, *1*, 144-158; doi:10.3390/rs1030144

OPEN ACCESS

Remote Sensing

ISSN 2072-4292

www.mdpi.com/journal/remotesensing

Article

Radiometric Calibration of Terrestrial Laser Scanners with External Reference Targets

Sanna Kaasalainen *, Anssi Krooks, Antero Kukko and Harri Kaartinen

Department of Remote Sensing and Photogrammetry, Finnish Geodetic Institute, Geodeetinrinne 2, 02431 Masala, Finland; E-Mails: Anssi.Krooks@fgi.fi (A.K.); Antero.Kukko@fgi.fi (A.K.); Harri.Kaartinen@fgi.fi (H.K.)

* Author to whom correspondence should be addressed; E-Mail: Sanna.Kaasalainen@fgi.fi; Tel.: +358-9-295 552 03; Fax: +358-9-295 552 00

Received: 2 June 2009; in revised version: 29 June 2009 / Accepted: 3 July 2009 / Published: 3 July 2009

Abstract: The intensity data produced by terrestrial laser scanners has become a topic of increasing interest in the remote sensing community. We present a case study of radiometric calibration for two phase-shift continuous wave (CW) terrestrial scanners and discuss some major issues in correcting and applying the intensity data, and a practical calibration scheme based on external reference targets. There are differences in the operation of detectors of different (although similar type) instruments, and the detector effects must be known in order to calibrate the intensity data into values representing the target reflectance. It is, therefore, important that the effects of distance and target reflectance on the recorded intensity are carefully studied before using the intensity data from any terrestrial laser scanner.

Keywords: terrestrial laser scanning; calibration; intensity

1. Introduction

Terrestrial laser scanning (TLS) has become a widely used remote sensing method, providing an effective and low-cost monitoring approach in many fields of research. Information on TLS performance and range data accuracy is constantly increasing [1,2], and this facilitates new fields of application and usage of existing instruments.

The use of TLS has gained wide attention in forest management and agriculture as an effective and non-destructive means of measuring, e.g., 3D-structure of trees and vegetation canopies (canopy gap fractions), tree volumes and leaf-area [3-5]. 3D modelling has become important in archaeology, e.g., building surveys and site models [6,7], where TLS is used to construct 3D models and create photo-realistic virtual copies of landscapes, buildings, and archaeological features (see also [8]). Furthermore, TLS has recently brought a new approach to geomorphological studies, providing effective and low-cost 3D site data, especially in hazardous and limited access areas, e.g., slopes with landslides [9] and permafrost affected rock walls in mountain regions, where rock falls occur and can be observed with TLS [10]. There is a growing interest in remote monitoring techniques in the study of the cryosphere, particularly in snow avalanche hazard regions, because of their inaccessibility and complications caused by these regions for traditional observation. Long-range (up to 2,500 m) laser scanners are usually preferred for this purpose [11,12]. In comparison of methods of snow depth determination for snowpack and snowdrift models, TLS has been found to be a quick means of getting high-point density data, having major advantages over manual probing, which is often time consuming and dangerous [13]. Integration of TLS and microwave ground-based SAR (synthetic aperture radar) data has also been studied in glaciology for measuring snow depth in mountainous regions [14].

TLS data has also been used in combination with airborne laser scanner (ALS) data or matched with digital images, to obtain, e.g., 3D city models for urban planning and virtual reality purposes [15,16]. Accurate 3D geometric information on real objects is also important in computer vision and robotics research to create virtual reality and digitally preserving cultural heritage objects. Range sensor (such as TLS) data merged with colour images provides an effective method for these applications [17,18].

One of the most recent and important future developments include vehicle-based (mobile) TLS, which has become a topic of increasing interest because of their high future potential for numerous different applications (see [19,20] for more references). Intensity calibration and correction procedure would be particularly important in mobile applications, where large distance/intensity variations have mixed effects on both of these parameters, and there are detectors that work differently at different distances. Only a small number of applications have been introduced thus far, such as monitoring the coastline, which is often difficult because of tides or the length of the coastline [21,22]. Furthermore, vehicle based systems are capable of faster and more effective data acquisition than the traditional stationary (multi-scan) laser scanning [21]. Further development and applications can also be expected in 3D city modelling (buildings and roads) [20,23], and agricultural studies [5].

In addition to the point cloud (x,y,z) data, most TLS instruments also record the point intensity value. The intensity measurement is mostly meant to enhance the range determination; therefore, the raw values of the intensity signal may be strongly modified by the instrument. There is usually no information on these modifications available without special requests to the manufacturer, let alone any calibration or correction methods of these values to get comparable intensity information. However, the use of TLS intensity data, also as reflectance information, is increasing, and knowledge on its reliability and correction methods have become an important topic of study and discussion. Mobile applications would especially benefit greatly from a possibility of calibration, similarly to airborne laser scanning (ALS), where the advantages of calibrated intensity have been more widely recognized to improve the accuracy of ALS data classification and many other aspects, such as target

recognition and change detection [24-26]. The potential of calibrated TLS intensity has been studied in snow cover change detection from intensity and range data, even though the accuracy of the intensity provided by TLS instruments would remain limited [27].

TLS intensity values have been mainly used as uncalibrated raw data. Even as such, they have found applications in, e.g., registering TLS data with digital camera images. This has become practical also because many of the TLS manufacturers offer a digital camera mounted on the TLS for simultaneous acquisition of high-resolution digital images [8,28]. The advantage of using calibrated intensity values as a reflectance image would be that in a one-shot intensity and point cloud data (x,y,z,I), there would be no need for georeferencing between separate data sets. Intensity information is also useful in extracting features (such as corners or edges of a building) from a TLS image (see [29] and refs. therein). There are also applications of intensity in the point cloud processing algorithms, such as scaling the point cloud images (e.g., [21]) and registration of point clouds from different scans [28]. Selection of points can also be made based on intensity, e.g., to separate foliage from wood in trees to generate tree skeletons and reconstruct branching structures [4]. Using the attenuation of TLS intensity in beam transmission provides a non-destructive means of tree-volume and leaf-area measurement in crop leaf area testing [5].

The effect of target intensity on the range accuracy has also been tested with retro-reflective targets: large errors occur in the distance measurement for highly reflective targets, resulting in errors if these targets are used in data georeferencing [30]. It has also been observed that intensity values which are too low influence the accuracy, and practically prohibit the range measurement [14]. Similar effects have been found for the range camera, which is also becoming popular in small-scale range measurement [31].

In spite of a variety of practical usage of intensity data, radiometric calibration of TLS intensity has become a topic of wider interest only recently, and few case studies have been published thus far [26,32]. The calibrated intensity has been applied, e.g., to the snow cover change detection [27]. Even though the same physical principles apply [25], there are some characteristics in TLS data acquisition and measurement that need special attention in putting the calibration methods into practise. The physical principles of laser scanner radiometric calibration are reviewed in, e.g., [25,33]. The basic idea in the radiometric calibration approach is to find a sequence of corrections that convert the instrumental (raw) intensity (or waveform) information into a value proportional (or equal) to target reflectance. This should be possible since, in principle, the received signal is proportional to the power entering the receiver, and hence to the reflectance. Since the measurement only occurs in one direction (backscatter), instead of the entire hemisphere of reflection, we can only measure a directional portion of the hemispherical reflectance, which we call here the *backscattered reflectance* of the target. How well the backscattered reflectance represents the full hemispherical reflectance properties of a target is a topic of further study; nevertheless, it is a value characteristic to the surface, and can be used in object classification and change detection from laser scanner data (see also [26]).

In this paper we discuss some important aspects of the radiometric calibration of TLS intensity data with the aid of a case study for two different TLS detectors for which there are fundamental differences in scaling and instrumental pre-processing of the intensity value. The concept of using external reference targets was first developed for ALS (e.g., [34,35]). In this paper we have extended this method to the radiometric calibration of stationary, continuous wave terrestrial laser scanners

(with no beam deflection pattern). Both brightness and distance scales are included in the study, because the effects of brightness and distance on the received signal seems to be somewhat mixed for TLS detectors. It is important that the effects of distance and target reflectance are well defined before making measurements and applying TLS intensity data.

2. Instruments and Data Correction

2.1. The Instruments and Measurements

One of the terrestrial scanners used in this study was the FARO LS HE80, which is a continuous wave 785 nm terrestrial laser. Phase modulation technique is used for the distance measurement; three different carrier wavelengths are modulated with an unambiguity range of approximately 76 metres. The distance measurement accuracy is 3-5 mm and the scanner field-of-view is 360° × 320°. The circular beam diameter at the exit is 3 mm and beam divergence 0.25 mrad. The laser power of the scanner is 22 mW, and the returning intensity is recorded in 11 bits [0 2048]. In 2009, the scanner was updated into Faro Photon 80, with 0.16 mrad beam divergence, and the distance error at 25 m reduced to 2 mm. The detector (photo multiplier) of the scanner is not designed for intensity measurement, but rather to optimise the range determination. Therefore, an amplifier for small reflectance has been added, which results in a logarithmic intensity scale. Additional correction of the intensity data is needed to get the raw intensity values into a linear scale. The detector is also equipped with a brightness reducer for near distances, which strongly affected the distance scale measurement.

Figure 1. The FARO Photon scanner and Fuji IS PRO camera mounted on a scissor lift rack, facing downwards. The samples are placed below the lift.

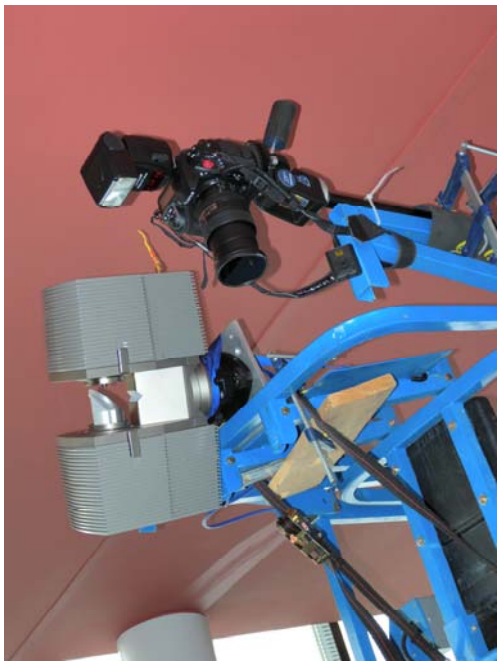

The second scanner used in this study was a Leica HDS6000, a 650-690 nm continuous wave laser scanner. A phase modulation technique similar to the FARO scanner is used for the distance

measurement, the unambiguity range being approximately 79 metres. The distance measurement accuracy is 4-5 mm and the field-of-view is 360° × 310°. The Leica scanner also has angular resolution selectable from full 0.009° down to 0.288°. The circular beam diameter at the exit and the beam divergence are 3 mm and 0.22 mrad, respectively. A silicon Avalanche Photo Diode (APD) is used as a photodetector.

The distance effect on the intensity data of these two scanners was studied by using a four-step Spectralon® (Labsphere Inc.) reflectance target of 12%, 25%, 50%, and 99% reflectance. The 99% panel was mainly used as a reference to calibrate the backscattered reflectance of other targets. FARO LS880HE was first tested in 2007 and after conversion to Faro Photon, the experiment was repeated in 2009. Leica HDS6000 was also tested in 2009. In 2009, we used profiler mode in both scanners to speed up the measurement process: the position of the scanner was stationary, and a four-step Spectralon was constantly moving away from the scanner, as opposed to have individual scan for all different distances (as in the FARO 2007 measurement, where the scans were made at 1-2 metre increments). In the profiler mode, only the reflection mirror (and not the scanner) rotates, but the technique has no effect on the measured intensity and range values. The angular effect was minimised by making an individual scan for all four planes of Spectralon, so that the each of the four sections was facing the laser beam directly. Intensity data was extracted from the resulting point clouds at 1 metre increments from 1 to 30 metres, which provided sufficient sampling to investigate the distance effects. The 30-metre maximum distance was chosen for practical reasons and the fact that our study was mainly focused on near distances (< 30 m).

A further study of the distance effect was carried out by mounting the FARO scanner on top of a scissor lift (Figure 1). The targets were then scanned in 50 cm increments (stationary mode) from about 2 m to 10 m height (the bounds were limited by the height of the lift rack and the ceiling of the building). The four-step Spectralon target was measured at each height, and the 99% Spectralon plate was used as reference. To investigate the distance effect on targets that represent airborne/terrestrial laser scanning land targets better than the Spectralon panel, we included some gravel samples in the measurement. This was also the reasoning for the use of the scissor lift, i.e., not having to tilt the samples in a vertical position as in the Spectralon distance measurements described above. Samples of crushed redbrick, beach sand from Kivenlahti beach, sanding gravel, and sandblasting sand (of 0.1-0.6 mm grain size) were also placed in the target field. The Kivenlahti beach has been an object of numerous ALS campaigns [35].

2.2. Data Correction

For both scanners, the raw intensity value of a surface was extracted by averaging points over a selected surface area in a point cloud image. From each target, a surface area as large as possible was sampled, so that for, e.g., a gravel sample, the area would not include any part of the container. The point cloud images were created using the standard software from the manufacturer (i.e., FARO Scene and Leica Cyclone). A point cloud image consists of the raw intensities recorded buy the detector. The Spectralon 99% intensity value was extracted similarly. To correct the logarithmic amplifier effects of the FARO scanner, the average value was then calibrated into backscattered reflectance R(target) with the following equation:

$$R(\text{target}) = 10^{(\frac{I(\text{target})}{I(\text{STD})} - A)/B} \quad (1)$$

where I(target) and I(STD) are the (raw) intensities of the target and and Spectralon 99%, respectively. A and B are constants pre-determined by a measurement of reflectance greyscale targets for the logarithmic correction (see [26] for more details).

The intensity values for the Leica HDS6000 scanner seemed linear in several tests with e.g., a four-step Spectralon target and calibration frame for NIR-camera; therefore, no logarithmic corrections were needed. However, Z+F LaserControl 7.4.5 (Zoller+Fröhlich GmbH) software had to be used for the extraction of raw intensity, because of intensity normalisation implemented in the data by the Leica Cyclone 6 software at the pre-processing stage, which complicated the radiometric calibration, and no linear values could be acquired.

Figure 2. A Fuji camera NIR-image of the samples, taken from the scissor lift. The gravel samples are seen on the left and the 4-step Spectralon panel on the right side.

2.3. Near-Infrared Digital Camera

A near-infrared (NIR) digital camera system was also mounted in the scissor lift to get reference measurements of reflectance at different distances to the targets. The system has also been tested on ALS campaign sites to provide *in situ* reference data for ALS radiometric calibration [35]. The camera is a Fuji IS PRO with an 850 nm IR-filter and Nikon SB800 flash with output power variation of ± 2%. This enables imaging in constant illumination with a small margin of error. The Fuji IS Pro has a boosted NIR sensitivity. It uses a charge coupled device (CCD) imager with red-green-blue (RGB) colour filter array to produce colour images. At 850 nm, all colour channels have quite uniform response, so the green channel is used for intensity measurements because it has the largest number of pixels. The camera was mounted next to the scanner with lens facing downwards to the targets (Figure 1), and an image was taken at each height simultaneously with the FARO scan. Figure 2 presents a Fuji-image taken of all the targets during the lift experiment.

The 14-bit raw format images (ISO100, 1/250s exposure time) were exported into linear 16-bit tiff-images (using dcraw open source raw converter), images were corrected using a flat field image, and the green channel intensity values were recorded (using ImageJ software). The average error for the camera measurements was estimated from the standard deviations of five separate camera exposures to be about 2.5% for gravel and sand type samples as well as the Spectralon panels.

3. Results

3.1. Distance Effects

First we studied the effect of distance on the scanner intensity. Figure 3 presents the FARO raw data (normalised with the 1-metre intensity value of the 99% panel) as a function of distance (the 2007 measurement). The values are presented before and after the logarithmic correction described in Section 2.2 and Equation 1. Figure 4 presents the similar values obtained from the Leica 2009 measurement, normalised with the 99% panel at 4.5 m. Normalization was carried out for easier comparison of intensity levels, and therefore the brightest value (raw data) for the 99% panel was chosen in each case. No logarithmic correction was needed for Leica because of the linearity of the intensity data. The distance effects are similar for both scanners: the maximum intensity is produced at about 5 m distance, after which fading occurs. The increase in intensity between 1 m and 5 m distances is most likely due to the near distance brightness reducer in the FARO scanner. According to the manufacturer, the Leica detector should not have any reducing effects, but we observed a reducing effect similar to that of FARO at distances of less than 5 m.

According to the manufacturer's information, the digital value of the FARO intensity also depends on the parameters of the analogue to digital conversion and the logarithmic amplification (cf. Section 2.1). The exact conversion and amplification values of an individual scanner are not provided by the manufacturer, so each instrument needs a specific calibration procedure. This is more or less the case for the Leica scanner as well, since, according to the manufacturer of the detector, the intensity is strongly affected by the receiver optics at distances below 12 m. This means that each individual scanner has to be calibrated separately, and no general law on the intensity behaviour can be established until a number of instruments have been investigated. This is particularly the case for other type, such as pulsed, detectors, which have not been included in this study. Pulsed lasers, however, have been studied in the ALS case with promising results [34,35]. For these reasons, we have focused our study on the empirical correction of these effects rather than a physical study of them at this point.

Figure 3. FARO: 2007 distance measurement, no logarithmic calibration of the amplifier, relative to the raw intensity of the 99% Spectralon at 1 m distance (top panel). The same (2007) measurement with logarithmic calibration, and normalised with 99% Spectralon at 1 m distance (lower panel).

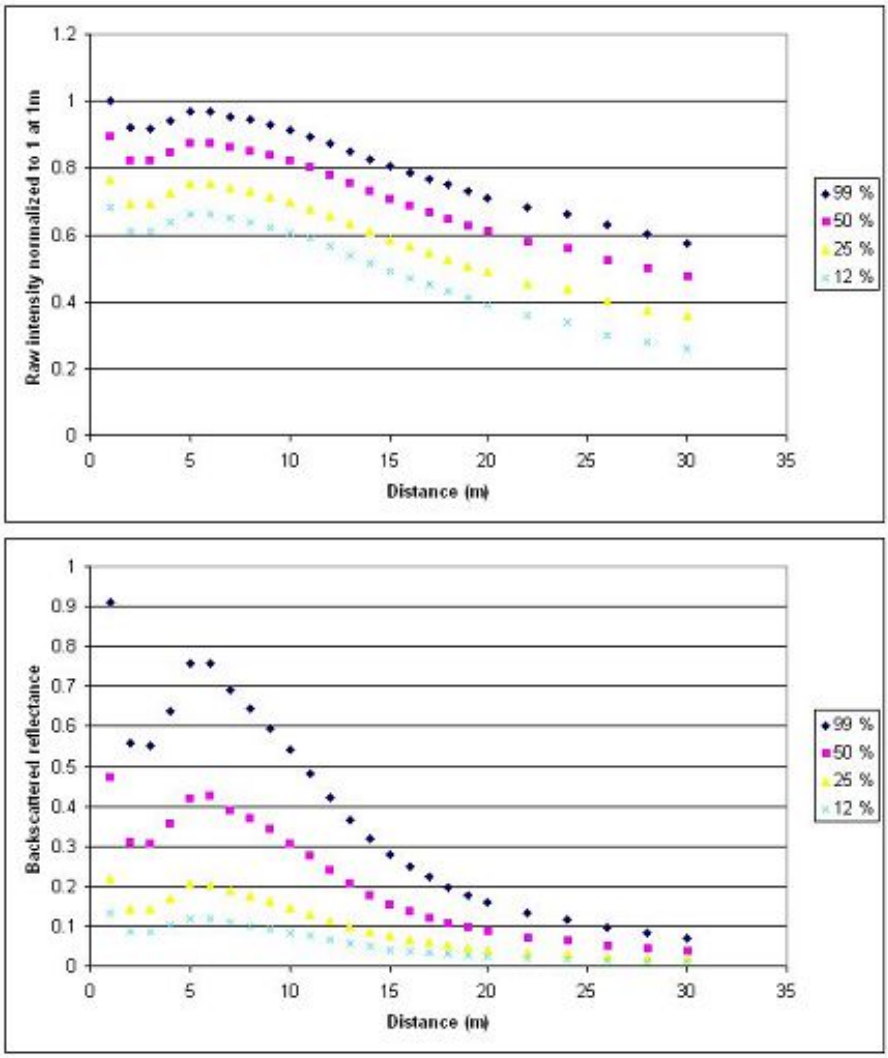

Figure 4. LEICA: 2009 distance measurement (profiler mode) normalised with 99% Spectralon standard at 4.5 m distance.

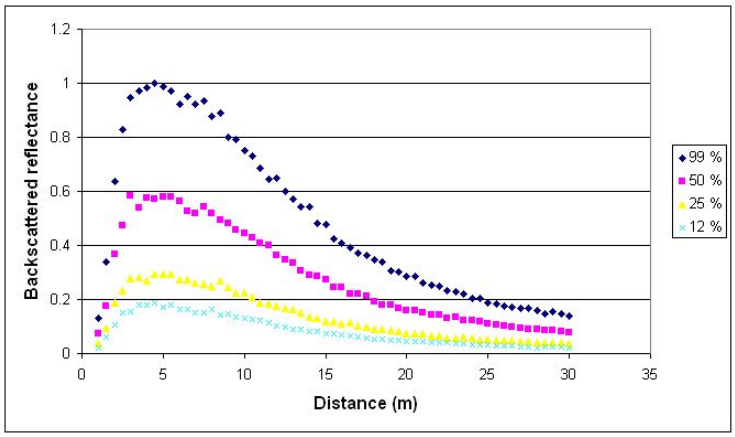

3.2. Calibration of Distance Effects

To investigate the feasibility of radiometric calibration and correction of the distance effect using a reflectance standard measured at the same distance to the target, we divided the 12%, 25%, and 50% panel intensities at each distance with the intensity of the 99% panel at the same distance. In Figures 5-7, both FARO and Leica results from 2007 and 2009 distance and scissor lift experiments are plotted. Note that the FARO reflectance levels are not repeated between experiments (2007 and 2009 distance measurement and the 2009 scissor lift experiment, Figures 5 and 6). This is also seen in Table 1. However, reflectance values from several field measurements in 2007 (i.e., before the upgrade into FARO Photon) are well in agreement with the 2007 distance measurement values: e.g., reflectance values at 4.2 m for the 25% and 12% Spectralon panels are about 0.22 and 0.13, respectively, from both the distance and field measurements. This indicates that the performance of the detector in the intensity measurement may have significantly changed in the scanner upgrade.

Table 1. Comparison of calibrated backscatter reflectance at about a 5 m distance with average errors (standard deviations). The average errors for the profiler mode experiments (FARO and Leica 2009) are estimated from stationary measurements for the same target. The 50% panel was used as reference for the Fuji measurements (because the 99% panel was poorly visible in the images).

	50% panel	25% panel	12% panel
FARO 2007, 5 m	0.494 ± 0.001	0.236 ± 0.001	0.134 ± 0.001
FARO 2009, 5 m	0.470 ± 0.002	0.207 ± 0.002	0.116 ± 0.002
Leica 2009, 5 m	0.59 ± 0.02	0.30 ± 0.02	0.17 ± 0.01
FARO/Lift, 5.2 m	0.553 ± 0.002	0.310 ± 0.002	0.196 ± 0.002
Fuji/Lift, 5.2 m	-	0.28 ± 0.09	0.18 ± 0.10

Furthermore, the distance effect is not corrected for FARO by using a standard at the same distance, and the effects of the small-reflectance amplifier and the near distance reducer are clearly visible in all three datasets: the reflectance values are not constant at distances less than 3 m, after which the nominal reflectance values of the three panels are not reproduced. The former is likely to be caused by the brightness reducer, whereas the latter may be due to the 99% panel being more strongly reduced by the brightness reducer than the other (lower reflectance) panels, but also because the target reflectance at backscatter may be different from the hemispherical (nominal) one. It is also likely that both the reducer and amplifier effects are mixed. The observed inconsistency also raises a question whether the amplitude modulation of the phase shift scanners affects the observed intensity, see [2] for more details on the phase shift technique. This means that the target may be illuminated differently at each range due to the interference of the modulated three waves. This, however, needs further investigation.

For the Leica, the distance effect is more consistent between different reflectance panels: the reflectance levels at different distances are constant, except for slight fading of the 12% and 25% targets over distance (Figure 7). The reflectance of the 50% panel appears noisier, because the curves (and hence the noise levels) are flattened for the other two targets plotted in the same scale. The

nominal reflectance values of the panels are not reproduced by the Leica scanner either, which may also be an effect of the measurement geometry. Similar reflectance levels have been produced by Leica in other experiments carried out in field conditions, with the Spectralon target placed some 2.0-2.5 m from the scanner, so the reflectance values produced by the Leica scanner seem repeatable.

The results from all measurements are compared in Table 1, where backscattered reflectance at a 5 m distance is compared for each panel. The 5-meter distance was chosen because we could assume the near-distance detector effects to be negligible at that distance. In spite of the slight wavelength differences between the different sensors used in this study, these results are comparable because the spectral variation for these targets has been previously measured to be small in the wavelength range spanned by these instruments [34].

Figure 8 presents the Fuji NIR camera results from the scissor lift experiment. Here the 50% panel was used as a reference for the Fuji measurements because, being in the edge of the image field, the 99% panel was not entirely visible in all images (cf. Figure 2). The intensity at 2.2 m was set to 0 because of this. The Fuji results at 5 m are also compared to the scanner reflectance in Table 1. The results are similar to the Leica results, i.e., there is little or no distance effect, even though some deviation in data exists. The difference between reflectance levels between the camera and the scanners is partly due to the differences in the measurement geometry. The agreement of the Leica and Fuji results also indicates the linearity of the Leica intensity measurement. Qualitatively, the FARO results from the scissor lift experiment (Figure 5) are also in reasonable agreement with the Fuji results, at least at scanner distances greater than 5 m.

Figure 5. FARO: 2009 scissor lift experiment results calibrated with the 99% Spectralon at the same distance as the target. The samples: crushed redbrick (denoted ‘Redbrick’ in the plot legend), beach sand from Kivenlahti (Beach), sanding gravel (Sanding), and sandblasting sand (Sandblast).

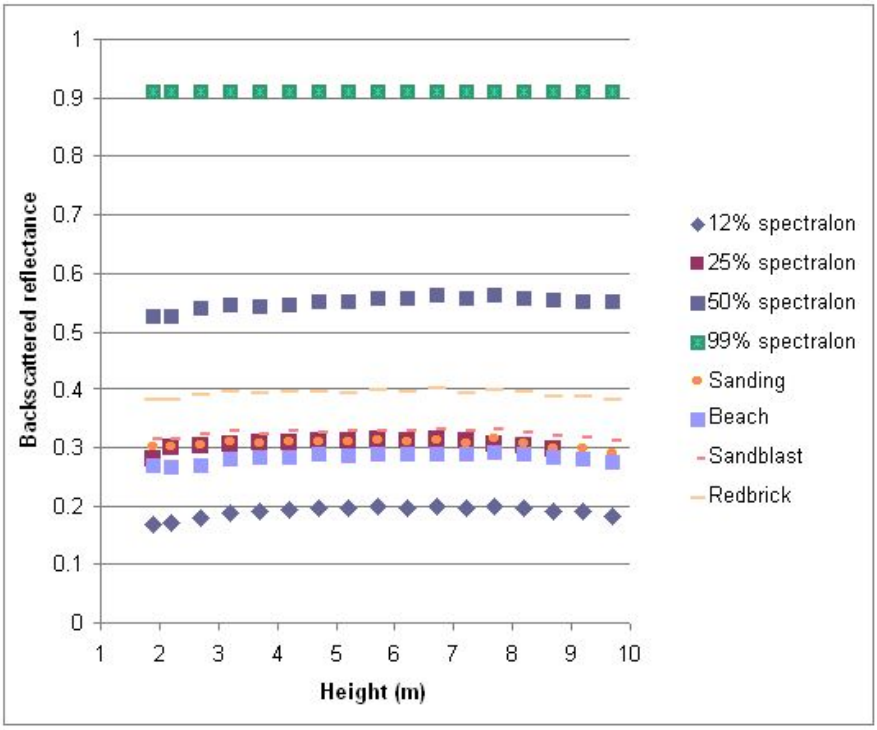

Figure 6. FARO: 2007 stationary (top) and 2009 profiler mode (bottom) distance measurement with logarithmic correction, and calibrated with 99% Spectralon at the same distance as the target.

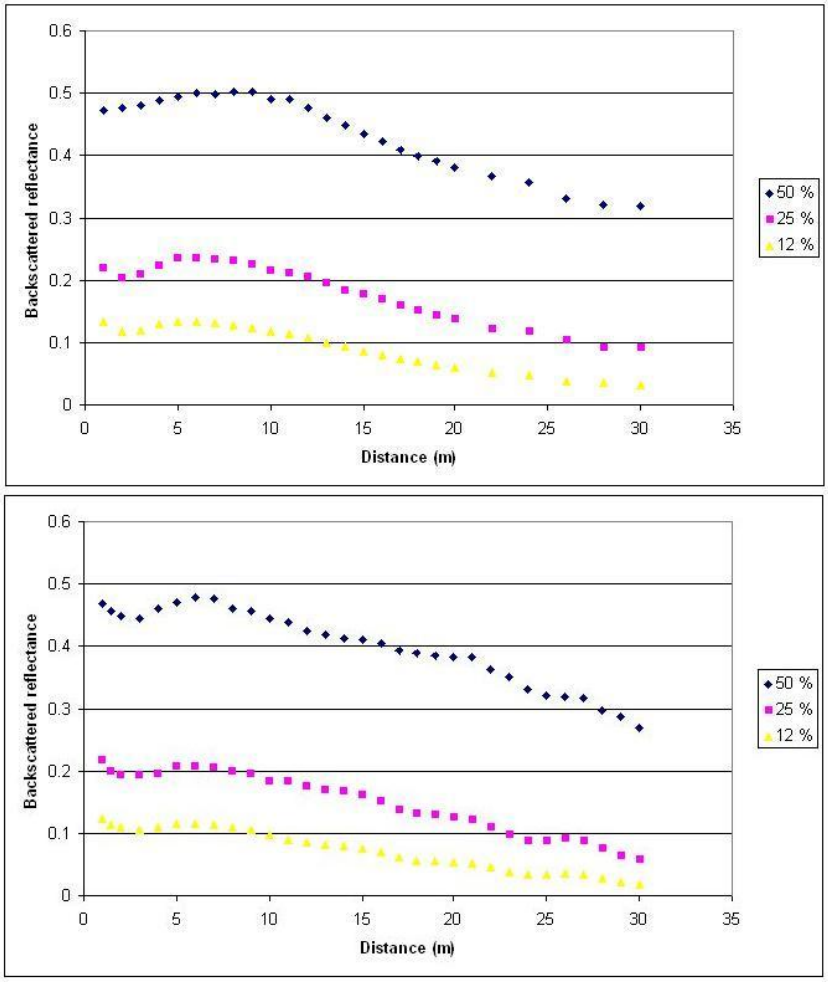

Figure 7. LEICA: 2009 distance measurement (profiler mode), calibrated with 99% Spectralon at the same distance as the target.

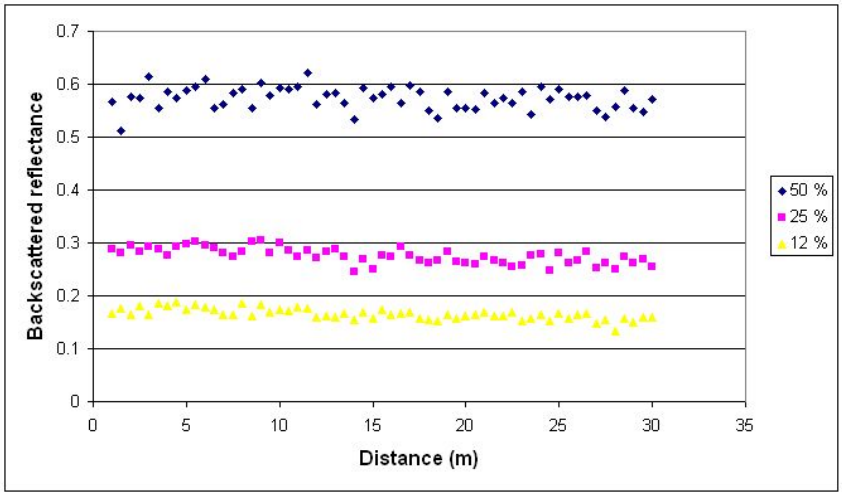

Figure 8. FUJI: 2009 scissor lift experiment, the same targets as for FARO (Figure 5).

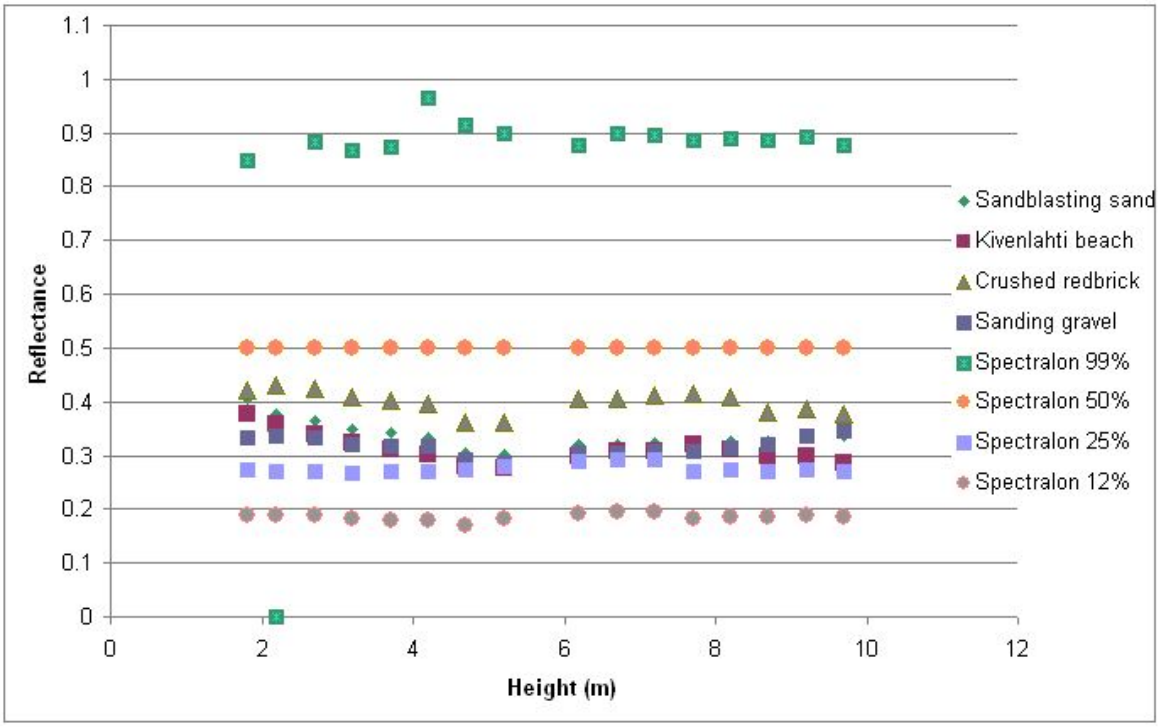

4. Conclusions

We have investigated the brightness and distance effects related to the radiometric calibration of FARO LS HE80 (later on FARO Photon 80) and Leica HDS6000 terrestrial laser scanners. Strong distance and brightness effects on FARO intensity data were observed, whereas for the Leica data, these effects are simpler and easier to calibrate using external reference targets. A NIR digital camera was used in the validation of these results, and it turns out that the camera-based approach seems useful for reflectance validation, especially in field conditions, where laboratory reference data are difficult to obtain in some cases (cf. [35]). Even though the intensity vs. distance behaviour of an individual scanner cannot be generalized at this point, the correction method with external reference targets can be applied, provided that there is enough information on the detector operation and characteristics.

In spite of differences between datasets, especially for the FARO Photon scanner, calibrated TLS data can be used in the development of classification and change detection methods, which are important in e.g., automatic target recognition procedures in mobile laser scanning, where large amounts of data are produced in a single data acquisition or campaign. Since the use of intensity information is becoming increasingly important in many applications, including those using a reducer/amplifier-based (nonlinear) detector, it is important to know the accuracy and limitations of the intensity data they produce and find methods for their calibration. This is particularly important in mobile applications.

Acknowledgements

The authors want to thank all the people who participated in these experiments: Hannu Hyyppä at Helsinki University of Technology, Ants Vain, Anttoni Jaakkola, Juha Hyyppä, and Eero Ahokas at FGI. This study was supported by the Academy of Finland (projects "Improving the applicability of intensity information in laser scanning" and "New techniques in active remote sensing: hyperspectral laser in environmental change detection").

References and Notes

1. Lichti, D.; Licht, M.G. Experiences with terrestrial laserscanner modelling and accuracy assessment. *Int. Arch. Photogramm. Remote Sens.* **2006**, *36*, 155–160.
2. Lichti, D.D. Error modelling, calibration and analysis of an AM–CW terrestrial laser scanner system. *ISPRS J. Photogramm. Remote Sens.* **2007**, *61*, 307–324.
3. Danson, F.M.; Hetherington, D.; Morsdorf, F.; Koetz, B.; Allgöwer, B. Forest canopy gap fraction from terrestrial laser scanning. *IEEE Trans. Geosci. Remote Sens.* **2007**, *4*, 157–160.
4. Côté, J.-F.; Widlowski, J.-L.; Fournier, R.A.; Verstraete, M.M. The structural and radiative consistency of three-dimensional tree reconstructions from terrestrial lidar. *Remote Sens. Environ.* **2009**, *113*, 1067–1081.
5. Rosell Polo, J.R.; Sanz, R.; Llorens, J.; Arnó, J.; Escolà, A.; Ribes-Dasi, M.; Masip, J.; Camp, F.; Gràcia, F.; Solanelles, F.; Pallejà, T.; Val, L.; Planas, S.; Gil, E.; Palacín, J. A tractor-mounted scanning LIDAR for the non-destructive measurement of vegetative volume and surface area of tree-row plantations: a comparison with conventional destructive measurements. *Biosyst. Eng.* **2009**, *102*, 128–134.
6. Al-kheder, S.; Al-shawabkeh, Y.; Haala, N. Developing a documentation system for desert palaces in Jordan using 3D laser scanning and digital photogrammetry. *J. Archaeol. Sci.* **2009**, *36*, 537–546.
7. Entwistle, J.A.; McCaffrey, K.J.W.; Abrahams, P.W. Three-dimensional (3D) visualisation: the application of terrestrial laser scanning in the investigation of historical Scottish farming townships. *J. Archaeol. Sci.* **2009**, *36*, 860–866.
8. González-Aguilera, D.; Muñoz-Nieto, A.; Gómez-Lahoz, J.; Herrero-Pascual, J.; Gutierrez-Alonso, G. 3D digital surveying and modelling of cave geometry: application to paleolithic rock art. *Sensors* **2009**, *9*, 1108–1127.
9. Dunning, S.A.; Massey, C.I.; Rosser, N.I. Structural and geomorphological features of landslides in the Bhutan Himalaya derived from Terrestrial Laser Scanning. *Geomorphology* **2009**, *103*, 17–29.
10. Rabatel, A.; Deline, P.; Jaillet, S.; Ravanel, L. Rock falls in high-alpine rock walls quantified by terrestrial lidar measurements: A case study in the Mont Blanc area. *Geophys. Res. Lett.* **2008**, *35*, L10502.
11. Prokop, A. Assessing the applicability of terrestrial laser scanning for spatial snow depth measurements. *Cold Regions Sci. Tech.* **2008**, *54*, 155–163.

12. Schaffhauser, A.; Adams, M.; Fromm, R.; Jörg, P.; Luzi, G.; Noferini, L.; Sailer, R. Remote sensing based retrieval of snow cover properties. *Cold Regions Sc. Tech.* **2008**, *54*, 164–175.
13. Prokop, A.; Schirmer, M.; Rub, M.; Lehning, M.; Stocker, M. A comparison of measurement methods: terrestrial laser scanning, tachymetry and snow probing for the determination of the spatial snow-depth distribution on slopes. *Ann. Glaciol.* **2008**, *49*, 210–216.
14. Luzi, G.; Noferini, L.; Mecatti, D.; Macaluso, G.; Pieraccini, M.; Atzeni, C.; Schaffhauser, A.; Fromm, R.; Nagler, T. Using a ground-based SAR interferometer and a terrestrial laser scanner to monitor a snow-covered slope: Results from an experimental data collection in Tyrol (Austria). *IEEE Trans. Geosci. Remote Sens.* **2009**, *47*, 382–393.
15. von Hansen, W.; Gross, W.; Thoennessen, U. Line-based registration of terrestrial and airborne LIDAR data. *Int. Arch. Photogramm. Remote Sens*. **2008**, *37*, 161–166.
16. Früh, C.; Zakhor, A. An automated method for large-scale, ground-based city model acquisition. *Int. J. Comput. Vision* **2004**, *60*, 5–24.
17. Stamos, I.; Allen, P.K. Geometry and texture recovery of scenes of large scale. *Comput. Vision Image Understand.* **2002**, *88*, 94–118.
18. Ikeuchi, K.; Oishi, T.; Takamatsu, J.; Sagawa, R.; Nakazawa, A.; Kurazume, R.; Nishino, K.; Kamakura, M.; Okamoto, Y. The Great Buddha project: digitally archiving, restoring, and analyzing cultural heritage objects. *Int. J. Comput. Vision* **2007**, *75*, 189–208.
19. Kukko, A.; Andrei, C.-O.; Salminen, V.-M.; Kaartinen, H.; Chen, Y.; Rönnholm, P.; Hyyppä, H.; Hyyppä, J.; Chen, R.; Haggrén, H.; Kosonen, I.; Capek K. Road environment mapping system of the finnish geodetic institute - FGI roamer. *Int. Arch. Photogramm. Remote Sens.* **2007**, *36*, 241–247.
20. Jaakkola, A.; Hyyppä, J.; Hyyppä, H.; Kukko, A. Retrieval algorithms for road surface modelling using laser-based mobile mapping. *Sensors* **2008**, *8*, 5238–5249.
21. Barber, D.M.; Mills, J.P. Vehicle based waveform laser scanning in a coastal environment. *Int. Arch. Photogramm. Remote Sens*. **2007**, *36*, C55.
22. Alho, P.; Kukko, A.; Hyyppä, H.; Kaartinen, H.; Hyyppä, J.; Jaakkola, A. Mobile TLS application for fluvial studies. *Geophys. Res. Abstr*. **2009**, *11*, 7601.
23. Amoureus, L.; Bomers, M.P.H.; Fuser, R.; Tosatto, M. Integration of LiDAR and terrestrial mobile mapping technology for the creation of a comprehensive road cadastre. *Int. Arch. Photogramm. Remote Sens*. **2007**, *36*, C55.
24. Coren F.; Sterzai P. Radiometric correction in laser scanning. *Int. J. Remote Sens.* **2006**, *27*, 3097–3104.
25. Höfle B.; Pfeifer N. Correction of laser scanning intensity data: data and model-driver approaches. *ISPRS J. Photogramm. Remote Sens.* **2007**, *62*, 415-433.
26. Kaasalainen S.; Kukko A.; Lindroos T.; Litkey P.; Kaartinen H.; Hyyppä J.; Ahokas E. Brightness measurements and calibration with airborne and terrestrial laser scanners. *IEEE Trans. Geosci. Remote Sens.* **2008**, *46*, 528–534.
27. Kaasalainen, S.; Kaartinen, H.; Kukko, A. Snow cover change detection with laser scanning range and brightness measurements. *EARSeL eProc.* **2008**, *7*, 133–141.
28. Kang, Z.; Li, J.; Zhang, L.; Zhao, Q.; Zlatanova, S. Automatic registration of terrestrial laser scanning point clouds using Panoramic Reflectance Images. *Sensors* **2009**, *9*, 2621–2646.

29. González-Aguilera, D.; Rodríguez-Gonzálvez, P.; Gómez-Lahoz, J. An automatic procedure for co-registration of terrestrial laser scanners and digital cameras. *ISPRS J. Photogramm. Remote Sens.* **2009**, in Press.
30. Pesci, A.; Teza, G. Terrestrial laser scanner and retro-reflective targets: An experiment for anomalous effects investigation. *Int. J. Remote Sens.* **2008**, *29*, 5749–5765.
31. Jaakkola, A.; Kaasalainen, S.; Hyyppä, J.; Akujärvi, A.; Niittymäki, H. Radiometric calibration of intensity images of SwissRanger SR-3000 range camera. *Photogramm. J. Finland* **2008**, *21*, 16–25.
32. Pfeifer, N.; Höfle, B.; Briese, C.; Rutzinger, M.; Haring, A. Analysis of the backscattered energy in terrestrial laser scanning data. *Int. Arch. Photogramm. Remote Sens.* **2008**, *37*, 1045–1052.
33. Wagner, W.; Hyyppä, J.; Ullrich, A.; Lehner, H.; Briese, C.; Kaasalainen, S. Radiometric calibration of full-waveform small-footprint airborne laser scanners. *Int. Arch. Photogramm. Remote Sens*. **2008**, *37*, 163–168.
34. Kaasalainen, S.; Hyyppä, H.; Kukko, A.; Litkey, P.; Ahokas, E.; Hyyppä, J.; Lehner, H.; Jaakkola, A.; Suomalainen, J.; Akujärvi, A.; Kaasalainen, M.; Pyysalo, U. Radiometric Calibration of LIDAR Intensity With Commercially Available Reference Targets. *IEEE Trans. Geosci. Remote Sens.* **2009**, *47*, 588–598.
35. Vain, A.; Kaasalainen, S.; Pyysalo, U.; Krooks, A.; Litkey, P. Use of naturally available reference targets to calibrate airborne laser scanning intensity data. *Sensors* **2009**, *9*, 2780–2796.

© 2009 by the authors; licensee Molecular Diversity Preservation International, Basel, Switzerland. This article is an open-access article distributed under the terms and conditions of the Creative Commons Attribution license (http://creativecommons.org/licenses/by/3.0/).